Supporting Information for

Surfactant-mediated Morphology Evolution and Self-assembly of Cerium Oxides Nanocrystals for Catalytic and Supercapacitor Applications

Xiaodong Hao[a,b,*], Shuai Zhang [a,c], Yang Xu[a,c], Liangyu Tang[b], Kazutoshi Inoue[b], Mitsuhiro Saito[d], Shufang Ma[a], Chunlin Chen[e], Bingshe Xu[a,*], Tadafumi Adschiri[b*], Yuichi Ikuhara[b,d,*]

[a]Materials Institute of Atomic and Molecular Science, Shaanxi University of Science & Technology, Xi'An 710021, China

[b]WPI-Advanced Institute for Materials Research, Tohoku University, Sendai 980-8577, Japan

[c]School of Materials Science and Engineering, Shaanxi University of Science & Technology, Xi'an 710021, China

[d]Institute of Engineering Innovation, the University of Tokyo, Tokyo 113-8656, Japan

[e]Shenyang National Laboratory for Materials Science, Institute of Metal Research, Chinese Academy of Science, Shenyang 110016, China

Table of Contents

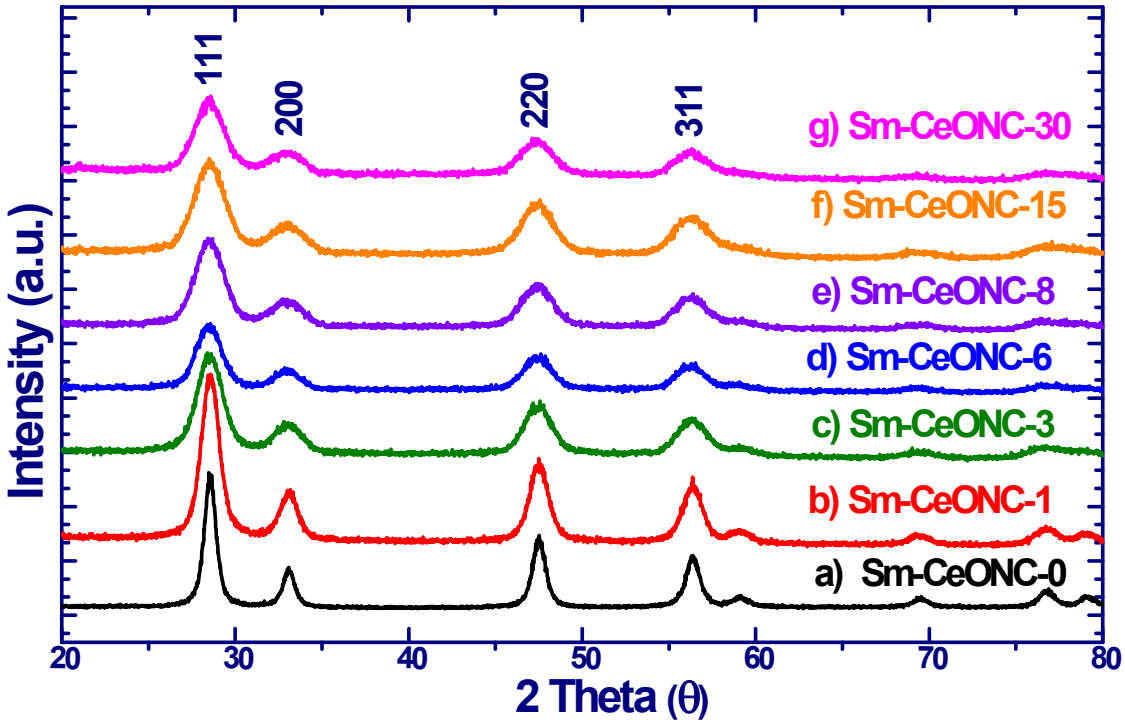

Figure. S1. XRD spectra of the as-synthesized Sm-CeONCs with different addition amount of surfactant.

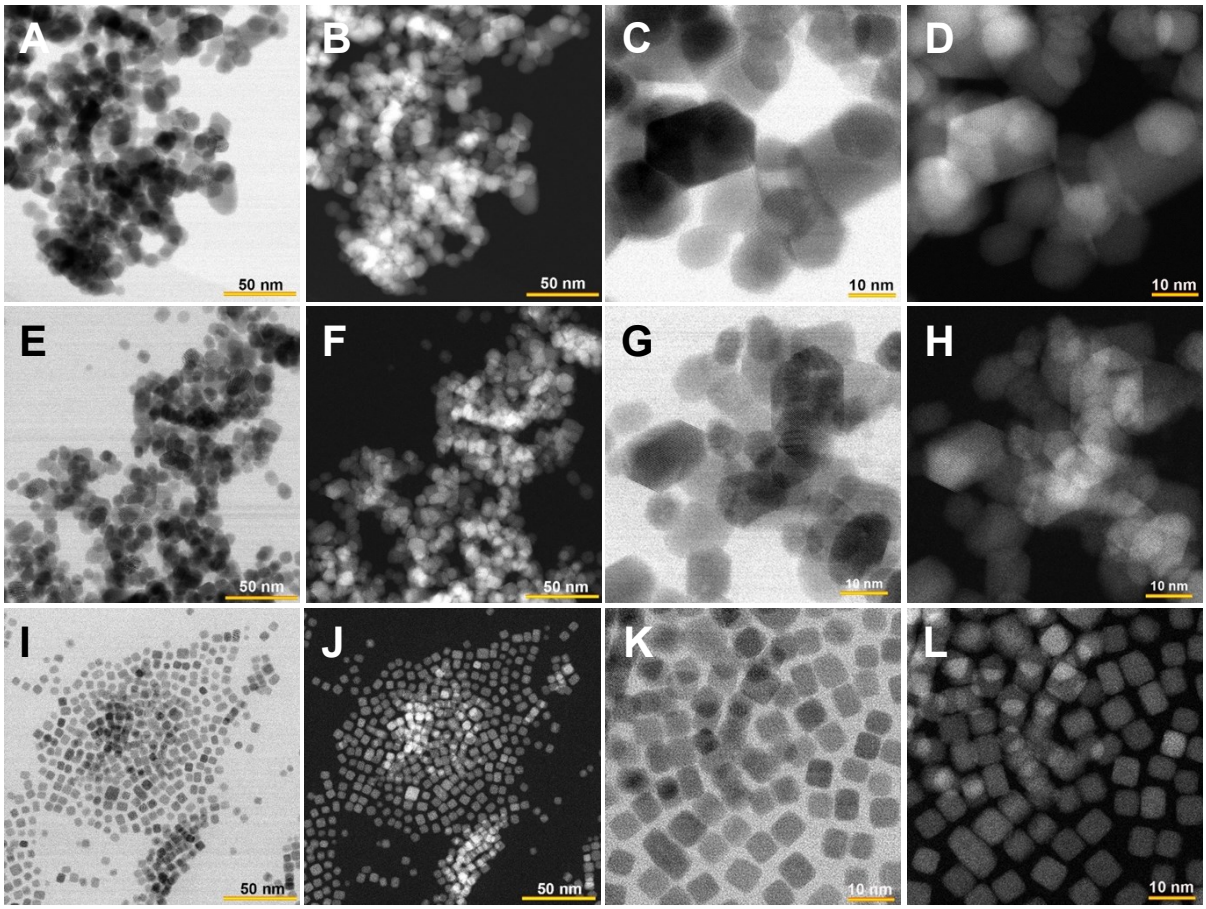

Figure S2. ABF- and HAADF images of (A-D) Sm-CeONC-0, E-H) Sm-CeONC-1, I-L) Sm-CeONC-2, respectively.

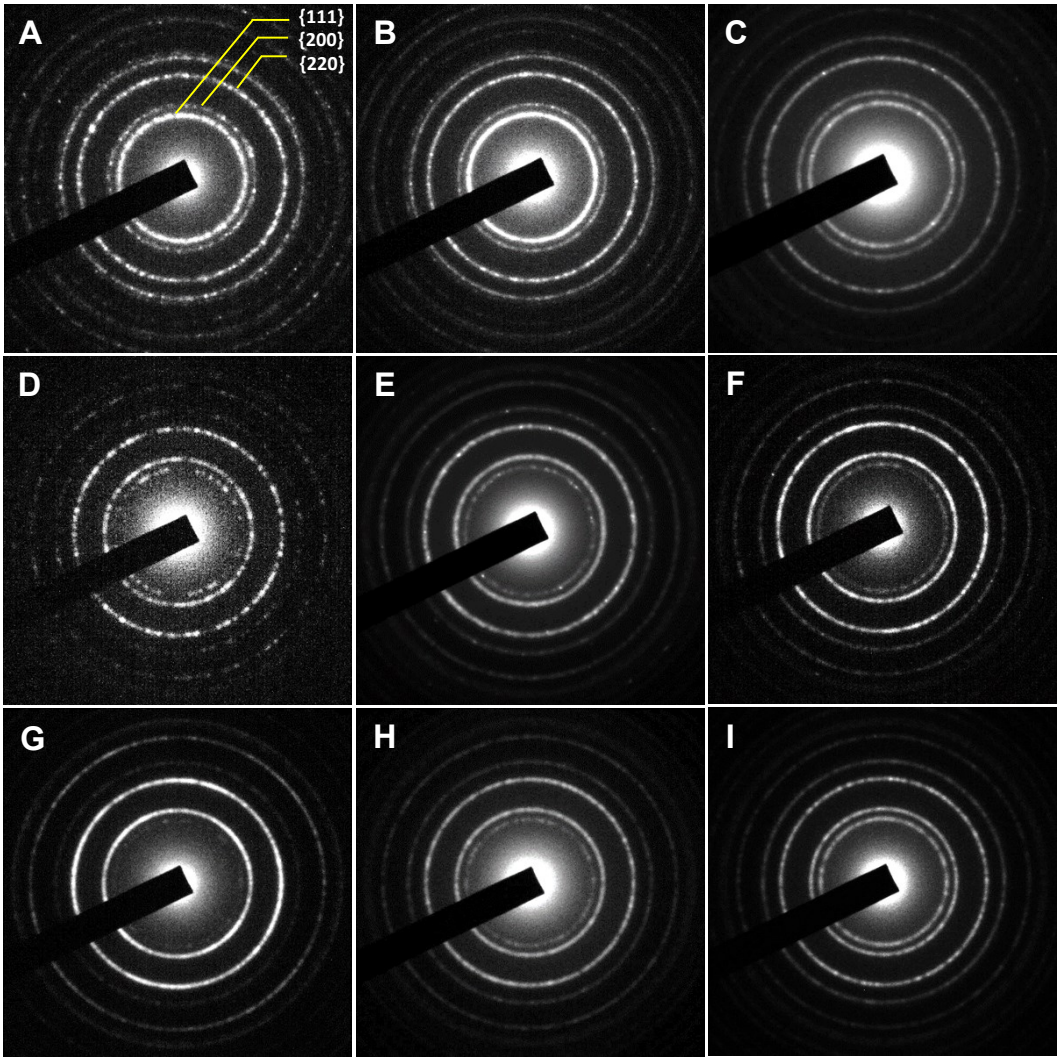

Figure S3. The corresponding selected area electrons diffraction patterns of the TEM images in Figure 2. The as-synthesized CeO_2 NCs with surfactant addition: A) Sm-CeONC-0, B) Sm-CeONC-1, C) Sm-CeONC-2, D) Sm-CeONC-3, E) Sm-CeONC-5, F) Sm-CeONC-6, G) Sm-CeONC-8, H) Sm-CeONC-15, I) Sm-CeONC-30, respectively. The camera length is 40 cm.

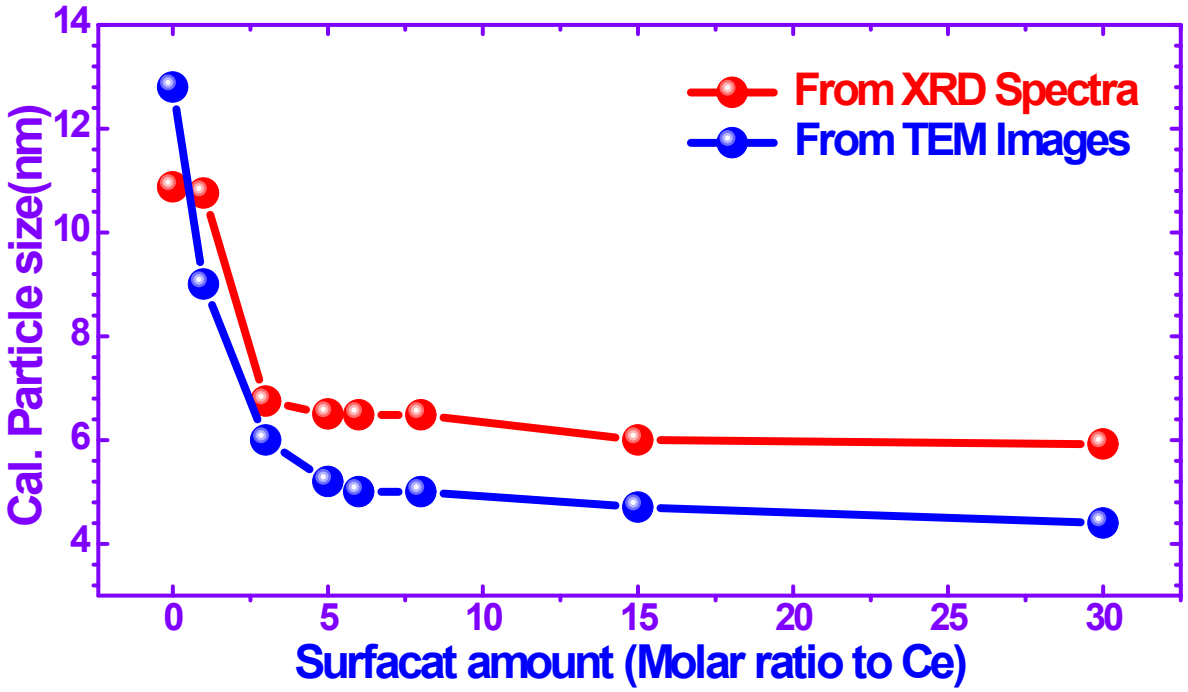

Figure. S4. Calculated NCs size of Sm-CeONCs with the different surfactant modification from TEM images and XRD spectra analysis.

The NCs size was calculated from the XRD data and TEM images. For the XRD spectra, Debye-Scherrer equation was used for the calculation, in which the full width at half maximum (FWHM) and exact diffraction angle was obtained from the Gaussian fitting process of the spectra. For the TEM images, Image-Pro Plus software was acquired for the statistical data of NCs size distribution. Both of these two calculation results showed the same trend of size decreasing with the increasing addition of surfactant.

Table S1. Facets fraction calculation according to the size and shape in this work.

Samples	Shape	Size (nm)	Facets fraction (%)		
			111	110	100
Sm-CeONC-1	Truncated octahedron	~11.0	**88.43**	**-**	**11.57**
Sm-CeONC-8	Cube	~6.5 nm	**0.62**	**17.18**	**82.20**
Sm-CeONC-30	Cuboctahedron	~5.0 nm	**33.60**		**63.40**

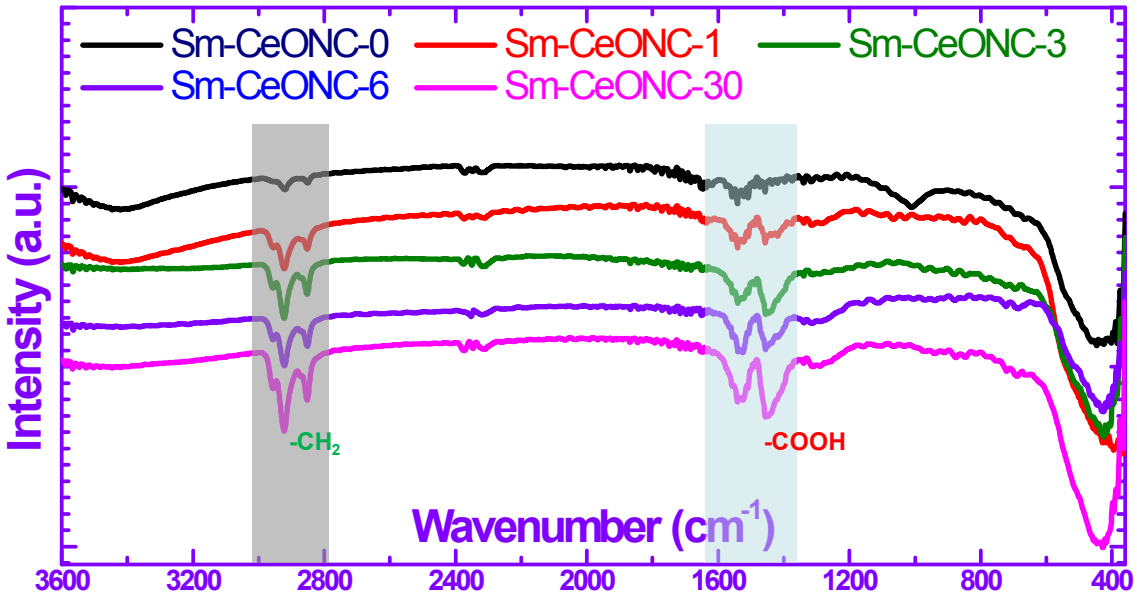

Figure S5. FTIR spectra of the representative samples of Sm-CeONCs with the different surfactant modification.

FT-IR spectra were taken for the confirmation on the existence of organic surfactant on CeO_2 NCs. The peaks in the 2800-3000 cm^{-1} region are attributed to the C-H stretching modes of methyl and methylene groups. The two strong peaks at around 1535 cm^{-1} and 1438 cm^{-1} in all the samples are corresponding to the vibration of asymmetric(ν_{as}) and symmetric(ν_s) stretching frequency of the carboxylate group, respectively. Previous reports studied the coordination between the carboxylic acid ($-COO^-$) and surface metal cations in the oxides by using the wavenumber separation Δ between the vibration bands of ν_{as} and ν_s: that is, chelating bidentate ($\Delta < 110$ cm^{-1}), bridging ($110 < \Delta < 140$ cm^{-1}) and unidentate ($200 < \Delta < 320$ cm^{-1}). In this work, the values of Δ for all the tested samples are < 100 cm^{-1}, indicating a chelating bidentate coordination type, that both the O from the carboxylic acid group are bonded with one surface cerium cation and the hydrocarbon chain is oriented outward [1-3].

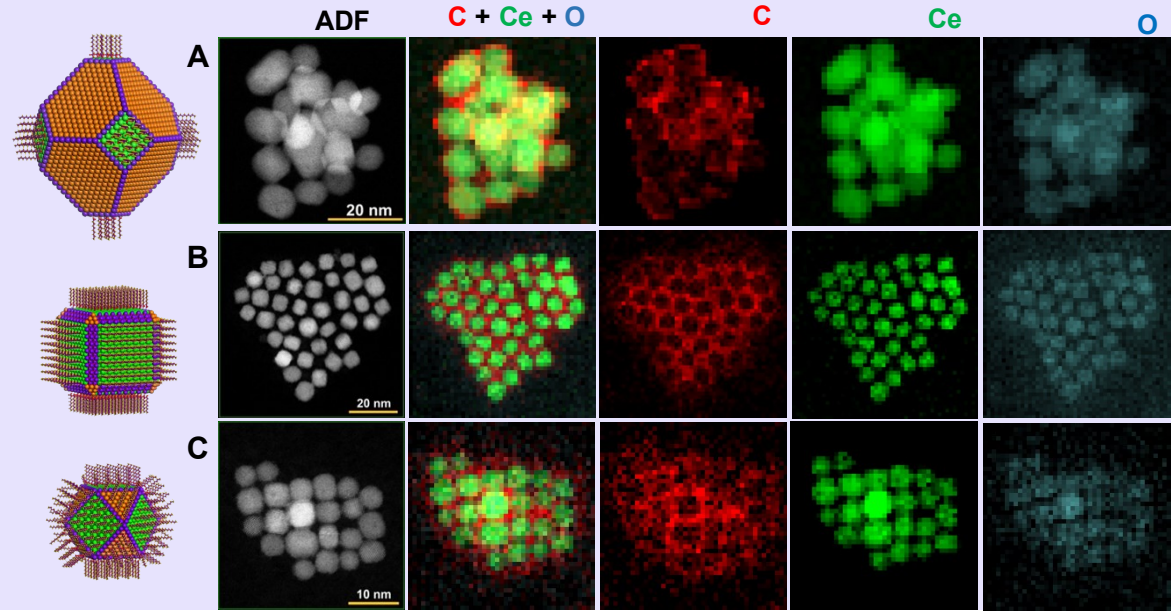

Figure S6. Direct determination of surfactant coverage on the representative samples of Sm-CeONCs by STEM-EELS. (A-C) Elemental mapping of (A) Sm-CeONC-1, (B) Sm-CeONC-8, C) Sm-CeONC-30, respectively. From the left to the right: raw ADF images, overlaid and separate elemental maps of carbon *K* edge (red), cerium *M* edge (green), and oxygen *K* edge (cyan), respectively. The NCs were deposited on silicon substrate and it was confirmed that the detected carbon signals were originated from the surfactant molecules as discussed in the previous report [4]. Models of surfactant modified CeO_2 NCs of a large truncated octahedron, cube and small cuboctahedron, as displayed in the left.

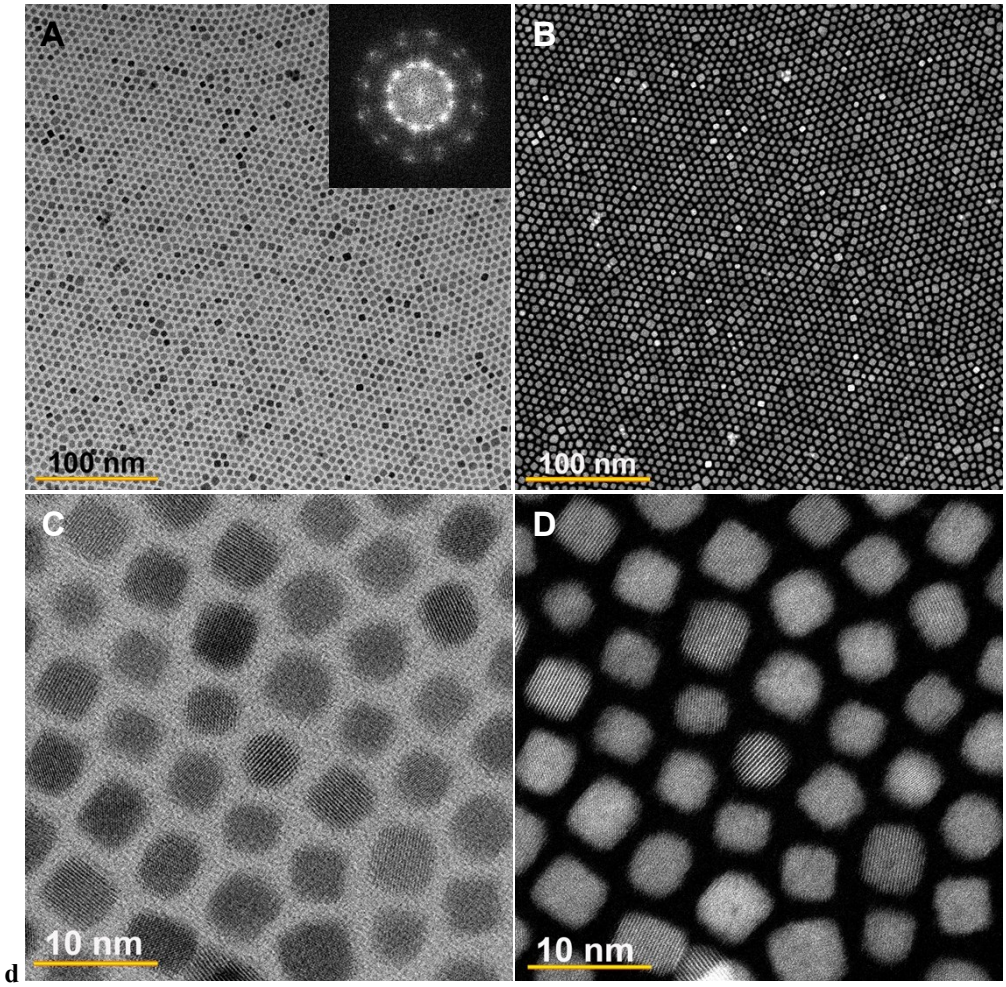

d

Figure S7. Self-assembly of cuboctahedra CeO_2 NCs. (A, C) ABF- and (B, D) HAADF-STEM images of cuboctahedra CeO_2 NCs (Sm-CeONC-30) superstructure.

The self-assembly of cuboctahedra CeO_2 NCs (Sm-CeONC-30) was also studied. As can be seen, because of the formation of small cuboctahedra NCs that the exposure of {111} facets was largely increased by excessive surfactant modification, the arrangement is changed that from 4-coordinated to 6-coordinated, as clearly shown in the atomic-scale ABF- and HAADF-image in Figure S6C and D. Thus, the FFT pattern from the low magnification ABF- and HAADF- images in Figure S6A and B also indicates a two dimensional NCs superlattice, which is different from that of cubic NCs superlattice in Figure 3A. This above difference can be easily interpreted if we deal with it by an analogy with the different projection of a face centred cubic (fcc) structure, that cubic NCs superlattice is from <011> direction, and the cuboctahedra NCs superlattice is from <111> direction.

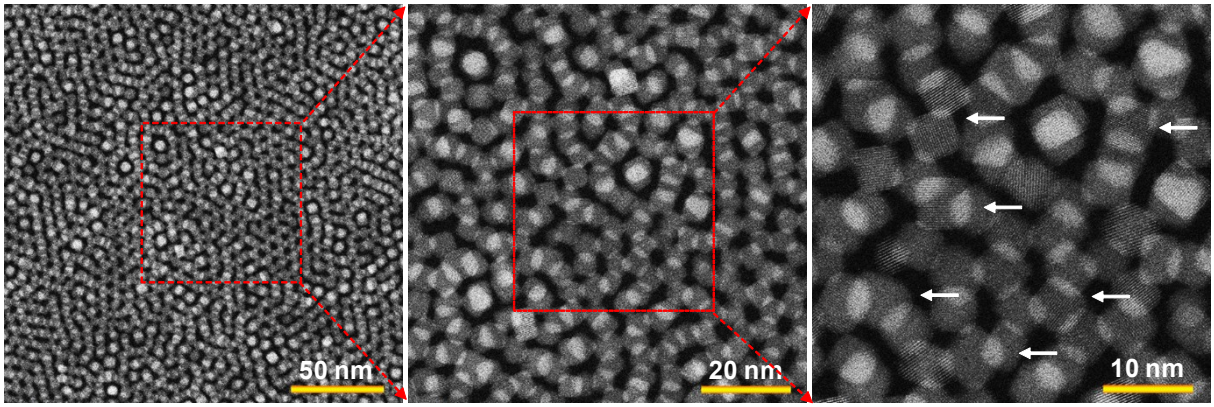

Figure S8. Self-assembly of multi-layers cubic CeO_2 NCs superstructure.

The formation of multi-layer cubic NCs ordered superstructures are also achieved in the densely distributed regions. The NCs in the top layer mostly locates atop the corners nearby NCs in the bottom layer, as indicated by the white arrow in the magnified HAADF image. It is also manifested that the {111} corners of NCs is not fully covered by the surfactant, so that the NCs in the top layers favours the location atop the NCs corners from the bottom layer to keep the stable arrangement.

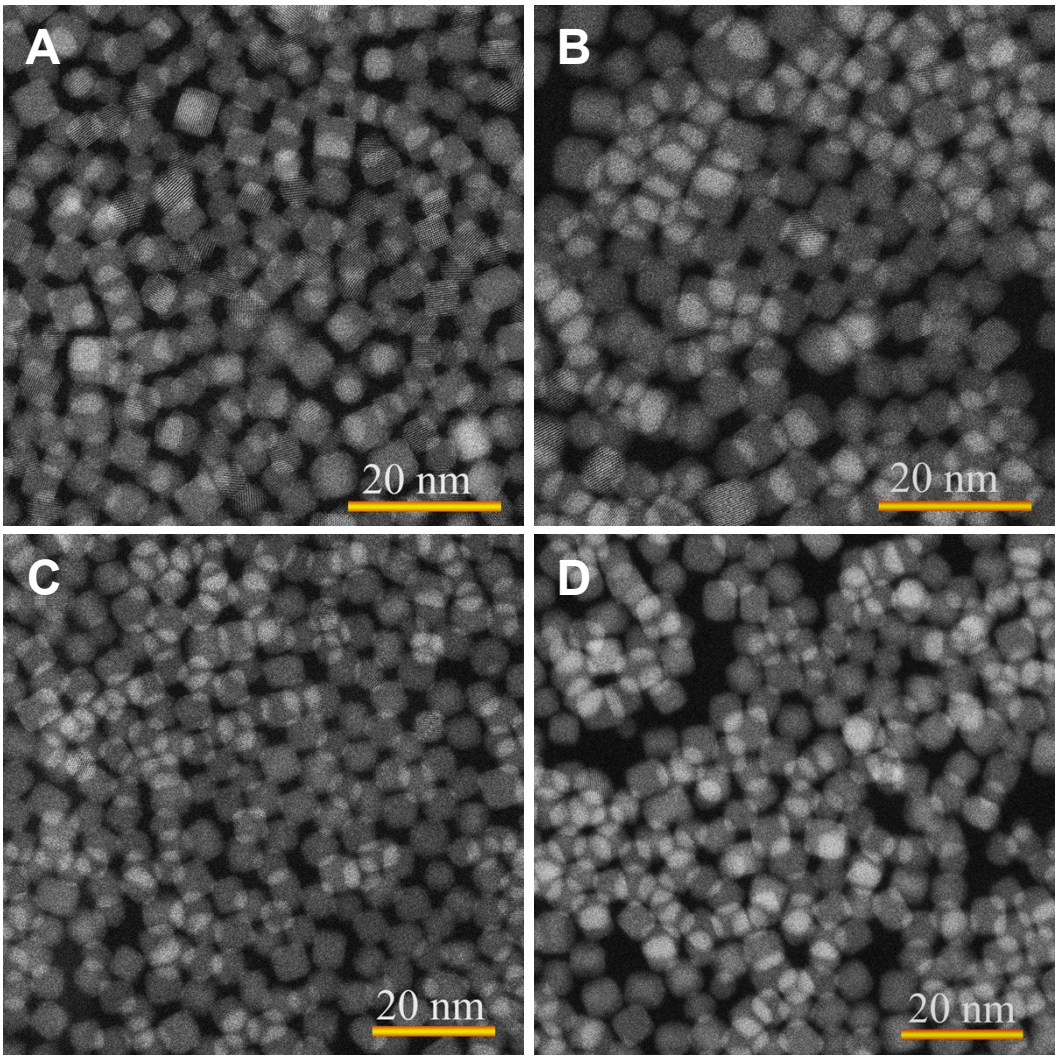

Figure S9. Thermal stability test of cubic CeO_2 NCs (Sm-CeONC-8) superstructures. (A-D) HAADF-STEM images of heat treatment of cubic CeO_2 NCs superstructures for 1 h in 200, 300, 400, and 500 ℃, respectively.

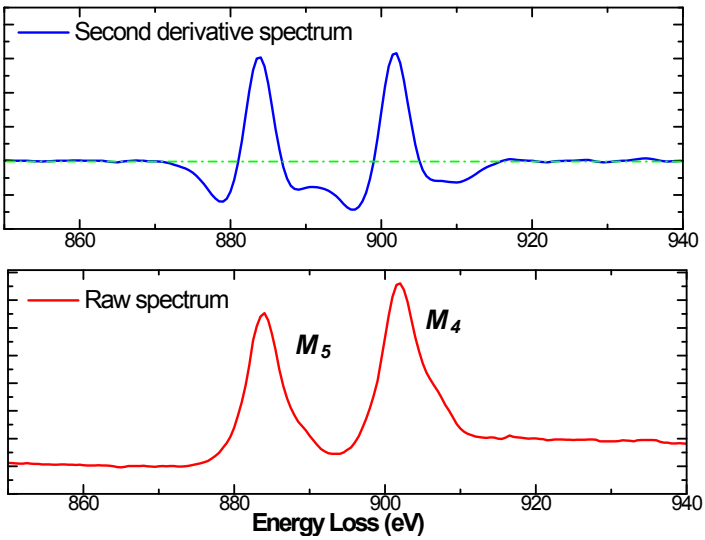

Figure S10. Second derivative method for the calculation of M_5/M_4 ratio.

A number of methods have been developed to measure the M_5/M_4 ratio, while the advantage of second derivative method over them is its insensitiveness to the energy resolution chosen and even the sample thickness. In this work, after the acquisition of Ce *M* edge spectra (bottom, in red), the corresponding second derivative spectra (up, in blue) is obtained by using the DigtalMicrograph software. Then the positive part of the M_5 and M_4 peaks in the second derivative of the spectra (above the green dot line) is measured using the script of "Measure the EELS peak intensities", subsequently the M_5/M_4 ratio is obtained. It is reported that the linear relationship exsiting between M_5/M_4 ratio and Ce valence state, and the using the reference value is summaried to be 1.31 for Ce^{3+}, and 0.91 for Ce^{4+}, particularly for the nanoparticles.[5-8] Therefore, the fraction of Ce^{3+} can be calculated from the formula listed below:

$$f = (M_5/M_4 - 0.91)/(1.31 - 0.91)$$

So, in this work, the M_5/M_4 ratio is 0.9954, 1.1530, 1.1281 for Sm-CeONC-1, Sm-CeONC-8, and Sm-CeONC-30, respectively. Therefore, the cubic CeO_2 NCs show the highest concentraton of Ce^{3+} of 60.74%, comparing to 21.34% in truncated octahedra and 54.52%.

Table S2. OSC performance of the as-synthesized Sm-CeONCs and CeO_2-CP commercial powders, respectively.

Temperature (℃)	CeO_2-CP	Sm-CeONC-1	Sm-CeONC-3	Sm-CeONC-6	Sm-CeONC-8	Sm-CeONC-30
200	0.3	10.0	16.8	24.2	16.3	11.9
300	0.4	174.1	215.5	257.5	273.0	290.2
400	2.5	183.3	255.6	319.5	364.6	355.5
500	25.6	252.2	455.6	534.2	620.1	638.0

Table S3. Comparison of the OSC performance of the as-synthesized Sm-CeONC-8 and Sm-CeONC-30 with other reported CeO_2 and CeO_2-based nanomaterials.

Catalytic materials	Temperature (℃)	OSC (μmol O/g)	References
Sm-CeONC-30	**500**	**638.0**	**This work**
Sm-CeONC-8		**620.1**	
CeO_2 tube	500	126	9
CeO_2 rod nanocrystals		84	
CeO_2 polyhedra		86	
CeO_2 cube		82	
Modified $Ce_{0.5}Zr_{0.5}O_2$ (CZ-1a)	400	320	10
Modified $Ce_{0.5}Zr_{0.5}O_2$ (CZ-2a)		615	
Modified $Ce_{0.5}Zr_{0.5}O_2$ (CZ-3a)		350	
$Ce_{0.8}Zr_{0.2}O_2$ (CZ80)	430	280	11
$Ce_{0.15}Zr_{0.85}O_2$	500	396	12
Ce(13%)YSZ		508	
Pt(0.01%)$Ce_{0.25}Zr_{0.75}O_2$	600	410	13
Pr(16%)$CeZrO_x$	400	588	14
Co_3O_4/CeO_2	250	150	15
Au- Co_3O_4/CeO_2		400	
CeO_2-ZrO_2	400	294	16
Pd(1%)-CeO_2-ZrO_2-(5%)BaO		586	
5 mol% Hf-CeO_2	Low Temperature	806	17
3 mol% Zn-CeO_2		516	
Pd(5%)/CeO_2(41%)-ZrO_2-Al_2O_3	350	920	18
CeO nanoparticles	550	260	19
La-CeO_2 nanoparticles		1160	
Co-La-CeO_2 nanoparticles		1540	

Table S4. Comparison of the supercapacitor performance of the as-synthesized Sm-CeONC-30 and Sm-CeONC-30 with the reported CeO_2 and CeO_2-based nanomaterials in the electrolyte of KOH.

Electrode Materials	Current density (A g^{-1}) or Scan rates (mV s^{-1})	Specific capacitance (F g^{-1})	Potential window (V)	Electrolyte (KOH)	References
Sm-CeONC-30	**1 A g^{-1}**	**339.5**	**-0.1-0.5**	**6M**	**This work**
Sm-CeONC-8		**287.0**			
CeO_2 Nanocubes	5 mV s^{-1}	122.8	0-0.5	2M	[20]
CeO_2 nanorods	1 A g^{-1}	162.5	-0.1-0.45	3M	[21]
CeO_2 nanocubes		149.0			
MnO_2/CeO_2	0.5 A g^{-1}	274.3	-0.1-0.4	3M	[22]
CeO_2/Fe_2O_3 CNS	5 mV s^{-1}	142.6	-0.3-0.3	6M	[23]
CeO_2/N-doped rGE	2 mV s^{-1}	230	-0.2-0.5	6M	[24]
CeO_2 NC/RGO	2 A g^{-1}	282	0-0.5	3M	[25]
Hollow sphere CeO_2/MCNTs	1 A g^{-1}	420	0-0.5	6M	[26]
Mesoporous CeO_2-Zr	1 A g^{-1}	448.1	0-0.5	2M	[27]
MOF derived CeO_2	0.2 A g^{-1}	502	0-0.5	3 M	[28]

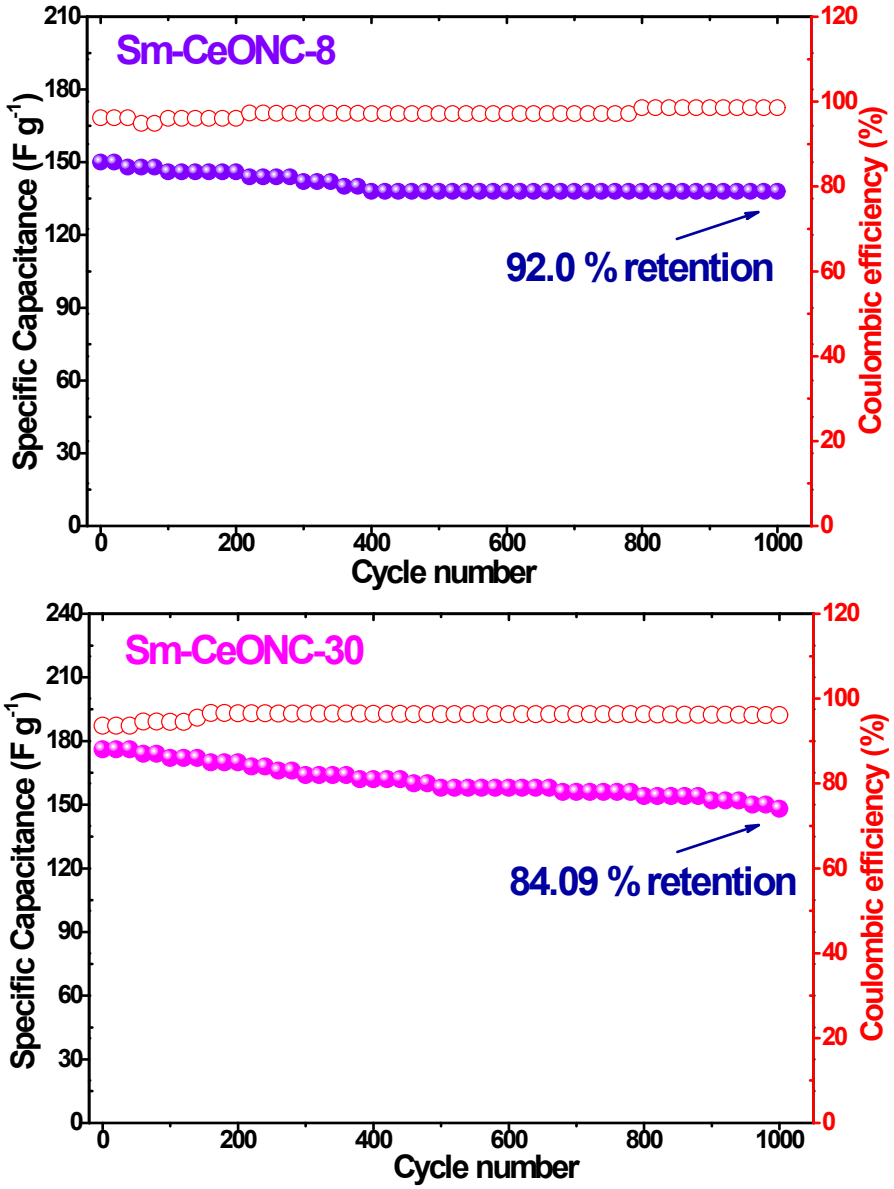

Figure S11. Variations of the capacitance and Coulombic efficiency with cycle number for Sm-CeONC-8 and Sm-CeONC-30.

References

[1] Deacon, G. B., Phillips, R. J., *Coordin. Chem. Rev.*, 1980, **33**, 227.
[2] Nakamoto, K., *Infrared and Raman spectra of inorganic and coordination compounds*, Wiley, New York, **1977**.
[3] Taguchi, M., Takami, S., Naka, T., Adschiri, T., *Cryst. Growth Des.*, 2009, **9**, 5297.
[4] Hao, X., Chen, C., Saito, M., Yin, D., Inoue, K., Takami, S., Adschiri, T., Ikuhara, Y., *Small*, 2018, **14**, 1801093.
[5] Fortner, J. A., Buck, E. C., *Appl. Phys. Lett.*, 1996, **68**, 3817.
[6] Wu, L., Wiesmann, H. J., Moodenbaugh, A. R., Klie, R. F., Zhu, Y., Welch, D. O., Suenaga, M., *Phys. Rev. B*, 2004, **69**, 125415.
[7] Hao, X., Yoko, A., Chen, C., Inoue, K., Saito, M., Seong, G., Takami, S., Adschiri, T., Ikuhara, Y., *Small*, 2018, **14**, 1802915.
[8] Hao, X., Yoko, A., Inoue, K., Xu, Y., Saito, M., Chen, C., Seong, G., Tomai, T., Takami, S., Shluger, A. L., Xu, B., Adschiri, T., Ikuhara, Y., *Acta Mater.*, 2021, **203**, 116473.
[9] Ju, T.-J., Wang, C.-H., Lin, S. D., *Catal. Sci. Technol.*, 2019, **9**, 2118.
[10] Li, J., Liu, X., Zhan, W., Guo, Y., Guo, Y., Lu, G., *Catal. Sci. Technol.*, 2016, **6**, 897.
[11] Sun, Y., Li, C., Djerdj, I., Khalid, O., Cop, P., Sann, J., Weber, T., Werner, S., Turke, K., Guo, Y., Smarsly, B. M., Over, H., *Catal. Sci. Technol.*, 2019, **9**, 2163.
[12] Arias-Duque, C., Bladt, E., Muñoz, M. A., Hernández-Garrido, J. C., Cauqui, M. A., Rodríguez-Izquierdo, J. M., Blanco, G., Bals, S., Calvino, J. J., Pérez-Omil, J. A., Yeste, M. P., *Chem. Mater.*, 2017, **29**, 9340.
[13] Kamiuchi, N., Haneda, M., Ozawa, M., *Catal. Today*, 2014, **232**, 179.
[14] Yang, X., Yang, L., Lin, S., Zhou, R., *J. Phys. Chem. C*, 2015, **119**, 6065.
[15] Gamboa-Rosales, N. K., Ayastuy, J. L., Gutiérrez-Ortiz, M. A., *Int. J. Hydrogen Energ.*, 2016, **41**, 19408.
[16] Yang, L., Yang, X., Zhou, R., *J. Phys. Chem. C*, 2016, **120**, 2712.
[17] Min, P., Zhang, S., Xu, Y., Li, R., *Appl. Surf. Sci.*, 2018, **448**, 435.
[18] Osaki, T., *Materials Research Bulletin*, 2019, **118**,
[19] Pizzolitto, C., Menegazzo, F., Ghedini, E., Innocenti, G., Di Michele, A., Cruciani, G., Cavani, F., Signoretto, M., *ACS Sustainable Chemistry & Engineering*, 2018, **6**, 13867.
[20] Chavhan, M. P., Som, S., Lu, C. H., *Materials Letters*, 2019, **257**, 126598.
[21] Jeyaranjan, A., Sakthivel, T. S., Molinari, M., Sayle, D. C., Seal, S., *Part. Part. Syst. Char.*, 2018, **35**, 1800176.
[22] Zhang, H., Gu, J., Tong, J., Hu, Y., Guan, B., Hu, B., Zhao, J., Wang, C., *Chem. Eng. J.*, 2016, **286**, 139.
[23] Arul, N. S., Mangalaraj, D., Ramachandran, R., Grace, A. N., Han, J. I., *J. Mater. Chem. A*, 2015, **3**, 15248.
[24] Heydari, H., Gholivand, M. B., *Applied Physics A*, 2017, **123**, 187.
[25] Li, T., Liu, H., *Powder Technology*, 2018, **327**, 275.
[26] Sun, Z. J., Ge, H., Zhu, S., Cao, X. M., Guo, X., Xiu, Z. H., Huang, Z. H., Li, H., Ma, T., Song, X. M., *J. Mater. Chem. A*, 2019, **7**, 12008.
[27] Sun, M., Li, Z., Li, H., Wu, Z., Shen, W., Fu, Y. Q., *Electrochim. Acta*, 2020, **331**, 135366.
[28] Maiti, S., Pramanik, A., Mahanty, S., *Chem. Comm.*, 2014, **50**, 11717.